

Estimation of Sintering Kinetics of Oxidized Magnetite Pellet Using Optical Dilatometer

T.K. SANDEEP KUMAR, NEELAKANTAN NURNI VISWANATHAN, HESHAM M. AHMED, CHARLOTTE ANDERSSON, and BO BJÖRKMAN

The quality of magnetite pellet is primarily determined by the physico-chemical changes the pellet undergoes as it makes excursion through the gaseous and thermal environment in the induration furnace. Among these physico-chemical processes, the oxidation of magnetite phase and the sintering of oxidized magnetite (hematite) and magnetite (non-oxidized) phases are vital. Rates of these processes not only depend on the thermal and gaseous environment the pellet gets exposed in the induration reactor but also interdependent on each other. Therefore, a systematic study should involve understanding these processes in isolation to the extent possible and quantify them seeking the physics. With this motivation, the present paper focusses on investigating the sintering kinetics of oxidized magnetite pellet. For the current investigation, sintering experiments were carried out on pellets containing more than 95 pct magnetite concentrate from LKAB's mine, dried and oxidized to completion at sufficiently low temperature to avoid sintering. The sintering behavior of this oxidized pellet is quantified through shrinkage captured by Optical Dilatometer. The extent of sintering characterized by sintering ratio found to follow a power law with time *i.e.*, Kt^n . The rate constant K for sintering was determined for different temperatures from isothermal experiments. The rate constant, K , varies with temperature as $\ln(TK^{1/n}) = \ln K' - \frac{Q}{RT}$, and the activation energy (Q) and reaction rate constant (K') are estimated. Further, the sintering kinetic equation was also extended to a non-isothermal environment and validated using laboratory experiments.

DOI: 10.1007/s11663-014-0273-y

© The Minerals, Metals & Materials Society and ASM International 2014

I. INTRODUCTION

IRON ores becoming leaner necessitate beneficiation at finer scales. Globally, this has led to growth in pelletization as an agglomeration process. In addition, pelletization of steel plant solid wastes enables them to be used in various iron and steel processes. Pelletization has been widely practiced for magnetite ores, as it offers an added advantage in terms of energy generated from the oxidation of magnetite to hematite. In Sweden, pelletization is the most important agglomeration process used industrially. Swedish steel industries have

stopped using the other widely used agglomeration process—sintering altogether and have pioneered in operating blast furnaces with cent percent pellets.

Magnetite ore grounded and beneficiated to an appropriate grade and size distribution is mixed with binder and agglomerated into spherical balls in a disk or drum pelletizer. The green pellets are strengthened through heat hardening process known as induration for subsequent use in iron making units such as blast furnace and direct-reduced iron processes. Induration is carried out in a straight grate furnace or in straight grate furnace followed by a rotary Kiln furnace. In straight grate, green pellets form a packed bed that is continuously moved through a long furnace. The hot gases are allowed to flow upward as well as downward through the packed bed for efficient heat transfer. In case of rotary Kiln process, partially processed pellets from a straight grate furnace are processed further in a rotating drum furnace. Pellet quality primarily measured in terms of strength and reducibility depends on the excursion the pellet makes through the thermal and gaseous environment in the induration furnace.

During induration, magnetite pellets undergo primarily drying, oxidation and sintering. Among these processes, drying almost gets completed at about 373 K (100 °C). Some of the chemically bonded water may not get released until the pellet temperature reaches 523 K (250 °C).^[1] At higher temperatures, primarily oxidation of magnetite and strengthening (sintering) occur.

Ideally for a good pellet quality, the oxidation of the pellet should be followed by sintering of the oxidized

T.K. SANDEEP KUMAR, Doctorate Student, and BO BJÖRKMAN, Chaired Professor, are with the Department of Civil, Environmental and Natural Resources (SBN), Lulea University of Technology (LTU), 97187 Luleå, Sweden. Contact e-mail: kamesh.sandeep@ltu.se NEELAKANTAN NURNI VISWANATHAN, Visiting Professor is with the Department of Civil, Environmental and Natural Resources (SBN), Lulea University of Technology (LTU), and also Professor with the Department of Metallurgical Engineering & Materials Science, Indian Institute of Technology Bombay (IITB), Mumbai 400076, India. HESHAM M. AHMED, Assistant Professor, is with the Department of Civil, Environmental and Natural Resources (SBN), Lulea University of Technology (LTU), and also with the Central Metallurgical Research & Development Institute (CMRDI), Cairo, Egypt. CHARLOTTE ANDERSSON, Specialist/Senior Researcher, is with the Oxidation Metallurgy, Research & Development, Luossavaara-Kiirunavaara AB (LKAB), Malmberget, 98381 Gällivare, Sweden.

Manuscript submitted August 18, 2014.

Article published online December 24, 2014.

magnetite grains.^[1,2] The oxidation determined by the intrinsic oxidation kinetics and diffusion of gases through the pores of the pellet proceeds from the pellet surface to the interior. This oxidation process is an exothermic process that generates heat within the pellet and can result in non-uniform temperature within the pellet. Simultaneously, the sintering of the oxidized magnetite (hematite) grains as well as the non-oxidized magnetite grains is initiated depending on the temperature and the sintering kinetics. It has been found that sintering of magnetite grains starts at much lower temperatures than that of hematite grains.^[1,3,4] Sintering, leading to a reduction of pore volume, adversely affects the oxidation phenomena. The interaction between oxidation, sintering, and the associated heat transfer can result in so-called duplex structure with a non-oxidized magnetite core with an oxidized shell.^[1,4-6] This interrelationship between various phenomena depends on the rate of these individual processes which in turn is determined by the processing conditions and the initial raw material.

In order to predict and quantify these physico-chemical phenomena during induration, a project has been initiated jointly by Lulea University of Technology (LTU) and Luossavaara-Kiirunavaara AB (LKAB). At present, models at the reactor scale exist for predicting the overall performance of the induration furnace. However, their ability to predict the quality of the pellets and its distribution is very limited.^[7-12] For realizing these objectives, it is important that the physico-chemical phenomena are quantitatively described at the pellet scale and subsequently can be used as an input to the models at the reactor scale. The methodology adopted is to study each of the aforementioned phenomena in isolation to the extent possible, quantify them and further integrate them through modeling techniques to understand the interaction among these phenomena. Such model can provide (1) building blocks for reactor scale models to predict pellet quality as a function of process parameters and (2) correlate the raw material quality in terms of content, additions, size distribution, *etc.*, to the induration process and pellet quality. These can help in designing process parameters for new grades of raw materials as well as improving existing processes. Sintering is one of the important phenomena during induration processes. The objective of this paper is to quantify the sintering of oxidized magnetite (hematite) pellet using optical dilatometer by deducing the kinetic parameters. Subsequently, the deduced kinetic parameters are validated with further experiments. Sintering kinetics of non-oxidized magnetite pellet will be presented in a future communication.

Powder metallurgists have been investigating sintering kinetics of the powder compacts of metallic and ceramic powders for many years.^[13-21] The extent of sintering of the powder compact is monitored through shrinkage measured using contact dilatometer. Numerous experiments have been reported on sintering studies on ceramic materials such as alumina, barium titanate, zirconia, uranium oxides, thorium oxides, *etc.*, as well as metallic materials such as Ti, Fe, Zr, stainless steel, *etc.*^[1,14,22-31] Traditionally, dilatometric measurements have been performed on briquettes having an alumina

push-rod to quantify shrinkage. The push-rod measures the linear displacement and cannot account for 2-D or 3-D spatial changes. A recent development by Expert System Solutions (ESS), Italy—Optical Dilatometer has facilitated to measure the dimensional variations solely on their optical images without having any contact with the sample. It works on principle of monitoring the periphery of the sample captured by two digital cameras equipped with high magnification and long working distance optical systems. Karamanov *et al.*^[32] compared the sintering kinetics estimated with the help of traditional push-rod dilatometer to that using the optical dilatometer. They found significant difference between these two measurements. They attributed the difference to the additional force exerted by the alumina push-rod over the sample contributing to its shrinkage. In this paper, a method to capture shrinkage of spherical pellets of approximately 10-mm diameter using Optical Dilatometer is established with an *in situ* measurement of area variation during sintering. This helps in assessing the shrinkage in 2-D. Any inhomogeneity in the green pellet can potentially get reflected in the shrinkage measurements.

Sintering is a complex process involving transport of species through various paths, such as bulk diffusion, surface diffusion, transport through the gaseous phase, *etc.*, driven primarily to reduce the total surface energy.^[33] Most of the studies in ceramic and metallic powder processing were focused in finding the predominant mechanisms operating at different extents of sintering and sintering temperatures.^[1,6,16,21,25,30,31,34,35]

Sintering studies on iron ore to deduce their kinetics have been relatively less. It can be noted that unlike conventional powder processing where the objective is to achieve close to 100 percent densification, in iron ore sintering, the objective is only to achieve sintering enough to provide sufficient strength during handling and subsequent operation in blast furnace and other reactors. At the same stage, sufficient porosity within in the pellet is necessary to achieve reduction in least time. Thus, sintering mechanisms responsible during the initial stages are only important for iron ore sintering. Wynnyckyj and Fahidy^[36] made an early in-road by studying the sintering kinetics of pure hematite reagent powder and commercial magnetite concentrate in the form of briquettes under isothermal conditions. They proposed a power law relation with time for isothermal sintering based on similar studies on sintering of metallic minerals and the same has been used in the present study. This model is described in detail at a later section. Interestingly, authors could not find any further quantitative studies either on magnetite or hematite sintering, though dilatometer measurements have been used to study sintering behavior.^[1]

II. EXPERIMENTAL DETAILS

A. Raw Material

The raw material chosen for the study was a concentrate from LKAB's Malmberget mine. It was preserved

Table I. Chemical Composition of Raw Materials

	Concentrate (wt pct)	Bentonite (wt pct)
Fe	71.06	3.63
SiO ₂	0.3994	51.64
CaO	0.1198	6.43
MgO	0.2596	0.68
ΣNa ₂ O + K ₂ O	0.078	3.30

carefully to avoid atmospheric moisture absorption. The concentrate contains Fe₃O₄ >95 pct with Al₂O₃ and SiO₂ <0.6 and 7 pct moisture by weight, as mentioned in Table I. The magnetite ore was ground in the open grinding circuit in ball mills in three stages to produce concentrate identified as Malmerget pellet concentrate (MPC) having fineness of 65 pct passing through 45- μ m screens and specific surface area \sim 9900 cm²/gm.

B. Balling

The concentrate was adjusted for humidity and then mixed with 0.5 pct dosage of bentonite as binder in a laboratory mixer (Eirich R02). This green mix of 7 kg was then fed to drum pelletizer (micro-balling) of 0.8-m diameter. Nucleation seeds of 3.5 to 5 mm were prepared first and subsequently balled into green pellets. The green pellets of desired size fraction of 9 to 10 mm were collected by screening. The smaller size of the green pellets than the widely used industrial average size (10 to 12 mm) for feeding into iron making units was decided based on the sample size limitations in the optical dilatometer (explained later). The green pellets were dried in oven at 423 K (150 °C) overnight, and stored in a desiccator for experiments.^[37]

C. Characterization

The pellets were characterized for their moisture content, true density, bulk density, and porosity. The known amount of green pellets were crushed and then placed into the Moisture Analyzer. Moisture analyzer completely evaporates the moisture by heating the sample overnight at 378 K (105 °C) and measures the weight loss. True density (skeletal density) of the single pellet as a whole was measured by AccuPyc II 1340 (Micromeritics Inc.) using 10 cm³ cell volume, the pycnometer which uses helium gas as displacement medium having an accuracy of 99.95 pct. The measurement of bulk density was tricky, as the use of commonly practiced Sand Flo pycnometer GeoPyc 1360 (Micromeritics Inc.) or Mercury Porosimeter would contaminate the surface of the pellet making it unsuitable for further processing. Therefore, use of tailor made light table imaging (LTI) was explored to measure the bulk volume of the pellet to determine its bulk density without harming the pellet surface. LTI is a set-up comprising high illumination light source, a high-resolution digital camera (Canon EOS 600D body with SIGMA lens of aperture 1:2.8), and software to capture the images for further analysis. This entire set-up is developed and synchronized by MBV Systems AB. 20 images of each

pellet at different angles and orientations were taken and analyzed using software ImageJ. The measurement of the bulk volume using this technique was calibrated using standard-sized dull luster spheres. The mean porosity of the pellet can be obtained from their bulk and true densities.

D. Oxidation

Magnetite pellet was well-nigh completely oxidized to hematite by placing them in a chamber furnace. During oxidation, pellet gains weight corresponding to degree of oxidation of 90 pct or more. The optimum oxidation temperature and holding time were obtained by performing experiments from 873 K to 1073 K (600 °C to 800 °C) at different time intervals over the period of 24 hours, and found them to be 1023 K (750 °C) and 4 hours, respectively. After achieving 90 pct oxidation at 1023 K (750 °C), the pellet does not undergo any substantial oxidation even after a prolonged holding time of 24 hours [87 to 97 pct when held for 2 to 24 hours, respectively, at 1023 K (750 °C)]. At temperatures lower than 1023 K (750 °C), the oxidation degree is very low whereas at higher temperatures sintering may happen, both of which was not desirable. The pellets were then allowed to cool to room temperature, and then transferred to optical dilatometer for subsequent processing.

E. Sintering

Sintering studies are performed on these oxidized magnetite pellets. Sintering captured in terms of shrinkage through a horizontal contactless optical dilatometer (Misura[®] HSM-ODHT), schematic of which is shown in Figure 1. It was programmed to measure area change as opposed to linear change by push-rod dilatometer. It comprises of three principal units mounted on an optical bench: a continuously illuminated halogen light source, a horizontal tube furnace (100 mm in length and 20 mm in diameter) which can go up to maximum of 1873 K (1600 °C) with a sample stage and an image capturing microscope with recording facility. It is equipped with double-beam optical measuring system having two lenses attached to the image capturing device—one compatible for small samples (2 to 5 mm diameter) whereas other for bigger samples (6 to 12 mm diameter). The microscope transfers the image of the sample in the furnace at 5 \times magnification through a quartz window and onto the recording camera. The pellet sample is placed on a small alumina plate (15 \times 15 mm²) resting on a thermocouple to measure the pellet temperature. It also has the provision for controlled in and out flow of the gases which maintains a constant flow across the pellet. The entire set-up is assembled to a computer system facilitated with specific Misura Thermal Analysis software to acquire and store the images of pellet subjected to a thermal profile, at predetermined time or temperature intervals. These images were processed to determine for area change as function of time during experiment.

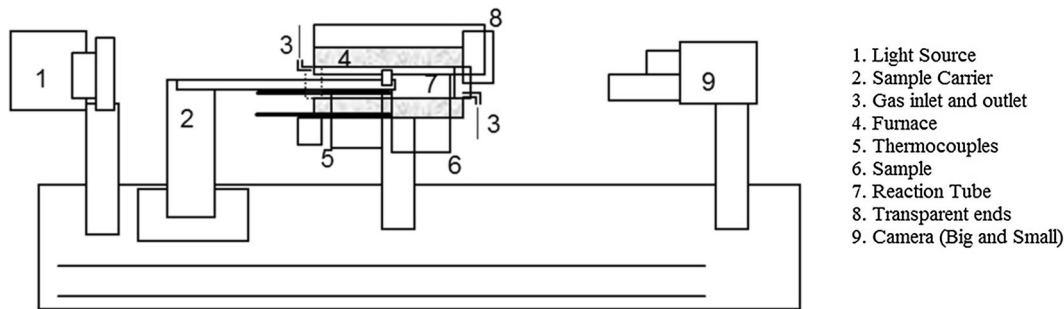


Fig. 1—Schematic of Optical Dilatometer (Misura® HSM-ODHT).

Table II. Experimental Design to Study Sintering Kinetics of Oxidized Magnetite

Pellet	Sintering Temperature [K (°C)]	Heating Rate [above 1073 K (800 °C)] [K/min (°C/min)]
P1	1423 (1150)	30
P2	1473 (1200)	30
P3	1523 (1250)	30
P4	1573 (1300)	30
P5	1623 (1350)	30
P6	1573 (1300)	15
P7	1573 (1300)	45

Pellets in all the experiments were exposed to a thermal profile of 50 K/min from room temperature to 1073 K (800 °C), and then at 30 K/min to the desired sintering temperatures as per experimental design mentioned in Table II, and holds at that temperature for 20 min. Experiments have also been conducted at different heating rates of 15, 30, 45 K/min reaching up to 1573 K (1300 °C) and subsequently holding the pellets isothermally for 20 min for the purpose of validation. Thereafter, the pellet was furnace cooled. A constant air flow rate has been maintained across the pellet in the furnace, so as to have sufficient oxygen available inside the furnace at any stage of sintering to avoid the dissociation of hematite back to magnetite. As the maximum flow rate specified for the optical dilatometer is 0.5 L/min, authors have used 0.3 L/min throughout which is within the maximum permissible limits. It has also been found that there is negligible change in weight before and after sintering assuring that the flow rate is optimum. The shadow images were captured continuously at an interval of 15 seconds to observe the shrinkage during sintering.

III. RESULTS AND DISCUSSION

A. Degree of Sintering and Sintering Rate

A typical plot showing the percentage area change, $\delta_{A, \text{overall}} = \frac{A - A_0}{A_0} \times 100$ for a pellet with respect to time following a thermal profile obtained is shown in Figure 2. It should be noted that 'A' refers to projected area of the pellet at any instant of time and 'A₀' refers to that at the start of the experiment. In these experiments,

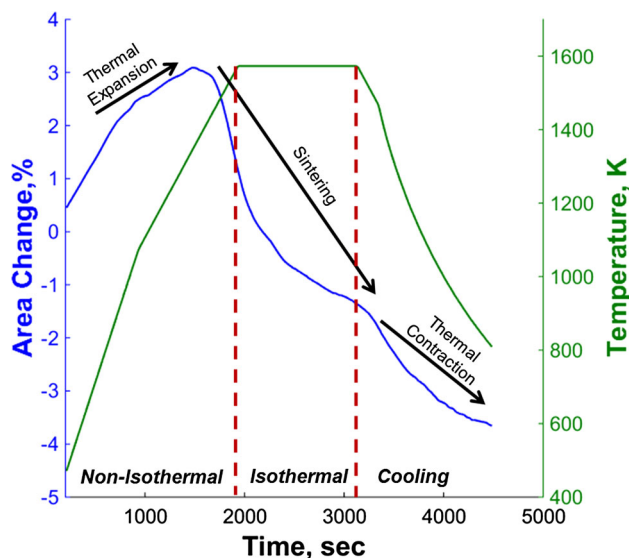


Fig. 2—Typical shrinkage curve obtained from Optical Dilatometer.

it has been assumed that the temperature of the pellet at any instant of time is uniform within whole pellet. In order to confirm this, preliminary experiments were conducted by embedding thermocouples at the center and at the surface of the pellet to measure the difference between surface and center temperatures, respectively, during heating of the pellet in a furnace. It did not show any significant difference at the center and the surface temperatures. This showed that the characteristic time for the center temperature to reach the surface temperature is very small as compared to that of sintering process. Therefore, it is reasonable to assume that the pellet has a uniform temperature throughout. These findings were also supported through analytical heat transfer calculations.

As shown in Figure 2, the pellet expands initially during induration, and after reaching a maximum it begins to shrink under the influence of thermal profile. Pellet undergoes thermal expansion, and once the temperature reaches around 1273 K (1000 °C), the sintering phenomena dominates resulting in overall shrinkage of the pellet. Shrinkage in the isothermal segment is due to sintering alone, and thereafter during cooling, the pellet continues to shrink because of thermal contraction as well.

Thus, the overall change in size of the pellet is due to the combination of the thermal expansion/contraction and the sintering phenomena. It is therefore, necessary, to isolate the thermal expansion/contraction phenomena from the overall percentage change in area to obtain the shrinkage due to sintering alone.

For this, the percentage change in area is plotted as a function of furnace temperature in Figure 3. It shows that the pellet expands linearly at low temperatures where sintering is insignificant, and as the temperatures goes beyond 1273 K (1000 °C) pellet begins to shrink non-linearly. During cooling also, the pellet shrinks linearly once the temperature reaches sufficiently low temperatures that the sintering is insignificant. The slopes of these linear variations both during heating and cooling are equal.

The volumetric thermal coefficient of expansion by its definition is given by,^[38]

$$\alpha = \frac{1}{V} \frac{dV}{dT}. \quad [1]$$

By integration,

$$\left(\frac{\Delta V}{V_0}\right) = \exp(\alpha(T - T_0)) \cong 1 + \alpha(T - T_0)$$

(Reasonable approximation for $\alpha \ll (T - T_0)$)

$$\text{or } \frac{V - V_0}{V_0} = \alpha(T - T_0). \quad [2]$$

In the above, V_0 is the initial volume of a material at temperature T_0 and V is volume of the material at any temperature T . Please note that, experimentally, the change in area is measured for the pellet and hence the area thermal coefficient expansion is expressed as

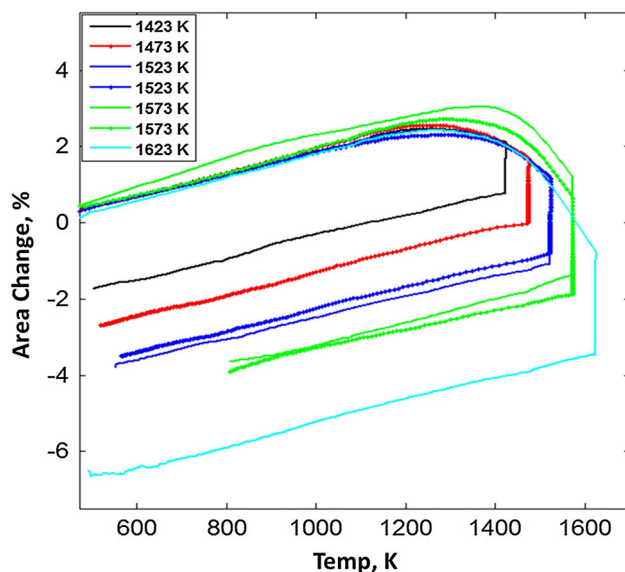


Fig. 3—Change in area with respect to temperature for pellets exposed to different sintering temperatures for estimation of thermal coefficient of expansion for iron ore concentrate.

$$\beta = \frac{1}{A} \frac{dA}{dT} = \frac{2}{3} \alpha. \quad [3]$$

The thermal expansion coefficient, thus estimated from Figure 3, aligns reasonably well with the reported values of pure magnetite. Using the estimated thermal expansion coefficient, the percentage area change due to sintering, $\delta_{A,\text{sintering}}$, was isolated from the overall change in area, $\delta_{A,\text{overall}}$. Subsequent analysis has been performed after isolating the percentage area change due to sintering alone ($\delta_{A,\text{sintering}}$).

Sintering is a thermally activated process, and hence the degree of sintering is expected to increase with increasing temperature. Figure 4 depicts the rate of sintering as a function time obtained for different sintering temperatures. Here, the rate of sintering increases with increasing temperature during non-isothermal heating due to enhancement in kinetics with increasing temperature. The rate of sintering decreases with time in the isothermal segment as the driving force for sintering progressively decreases with the extent of sintering. The driving force for sintering is the reduction in the surface area of grains in pellet which also results in reduction in pore volume. The rate of sintering is not only function of temperature but also the extent of sintering remaining (or the extent of sintering that has already occurred). Thus, at a constant temperature, as sintering progresses, the driving force available for further sintering reduces and hence the rate of sintering. It should be noted that experiments have also been repeated to ensure reproducibility of the results shown in Figure 4. Interestingly, the time at which the rate of sintering is the maximum seems slightly earlier than the start of isothermal segment. Authors are unable to explain this observation. Possibly this can be attributed to the temperature control system making a change from a constant heating rate to an isothermal segment.

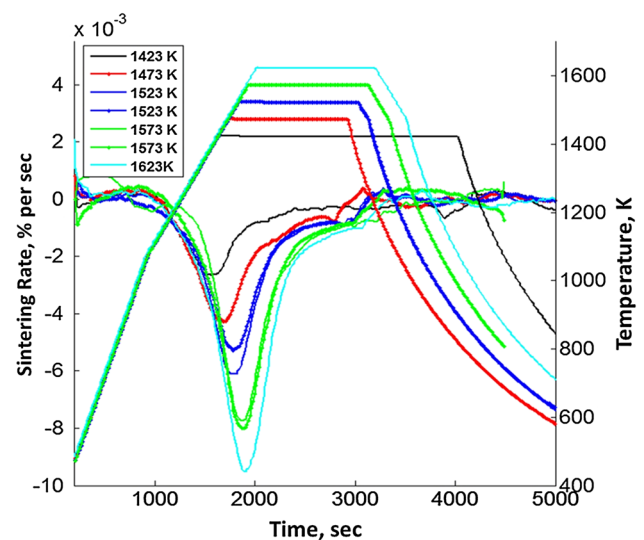


Fig. 4—Sintering rates for pellets exposed to different sintering temperatures.

B. Sintering Ratio (γ)

Wynnykyj and Fahidy^[36] had suggested that the sintering of material can be quantified by capturing its shrinkage and proposed a term sintering ratio (sintering extent). The sintering ratio for the pellet can be defined as the ratio of the sintering accomplished to the sintering yet to be accomplished:

$$\gamma = \frac{\text{Sintering accomplished}}{\text{Sintering yet to be accomplished}} = \frac{V_0 - V}{V - V_{\text{true}}}, \quad [4]$$

where V_{true} is the volume of the pellet if it would have undergone complete sintering with no pores remaining. The percentage change in area due to sintering, δ_A , can be defined in terms of bulk density of the pellet at any time, ρ , as

$$\delta_A = \frac{2}{3} \left[\frac{\rho_0 - \rho}{\rho} \right] \times 100 \text{ and } \delta_{A,\text{true}} = \frac{2}{3} \left[\frac{\rho_0 - \rho_{\text{true}}}{\rho_{\text{true}}} \right] \times 100. \quad [5]$$

The true density, ρ_{true} , of the solid constituents in the pellet is measured using Helium pycnometer having a standard deviation of 1 pct. From Eqs. [4] and [5],

$$\gamma = \frac{-\delta_{A,\text{sintering}}}{\delta_{A,\text{true}} + \delta_{A,\text{sintering}}}. \quad [6]$$

This equation relates the sintering ratio to the percentage area change measured.

C. Estimation of Sintering Kinetic Parameters

Wynnykyj and Fahidy^[36] proposed that the isothermal sintering kinetics can be expressed as

$$\gamma = Kt^n \quad [7]$$

where, t is the isothermal time, n is time exponent and K is reaction constant. It can be noted that the initial volume V_0 used in Eq. [4] correspond to start time ($t = 0$) when the pellet is in isothermal state. Further, the variation of reaction constant term, K , with respect to temperature was expressed using the following equation

$$\ln(TK^{1/n}) = \ln K' - \frac{Q}{RT} \quad [8]$$

Here, Q is the activation energy and K' is the sintering rate constant.

The variation in sintering ratio with time for different experiments is shown in Figure 5. In order to estimate the sintering kinetic parameters, the isothermal segment of the curve is used. However, as mentioned earlier, the time t given in Eq. [7] is the time starting from the instant if the pellet was kept under isothermal condition from the start. This was not so for the experiments wherein the isothermal segments were always preceded by non-isothermal section due to some constraints in the equipment. Therefore, an alternate methodology needs to be used to obtain the kinetic parameters.

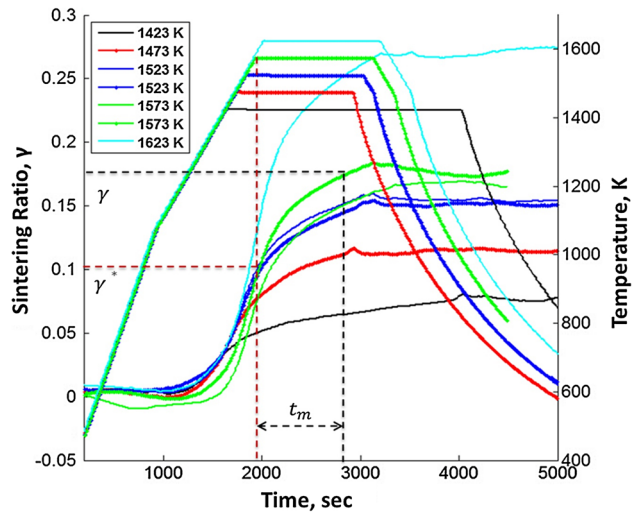


Fig. 5—Sintering ratio for pellets exposed to different sintering temperatures.

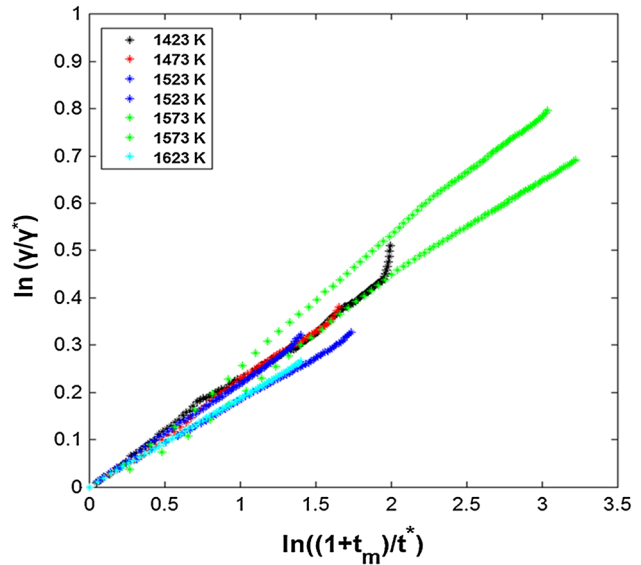


Fig. 6—Time exponent 'n' for oxidized magnetite pellets sintered at different temperatures.

Let us denote γ^* as the sintering ratio at the start of the isothermal section as illustrated in Figure 5. Thus, it is possible to define a time, t^* , which corresponds to a time if the pellet had attained a sintering ratio of γ^* from the start under isothermal condition.

If so, one can write Eq. [7] as

$$\gamma^* = K(t^*)^n$$

and beyond t^* ,

$$\gamma = K(t^* + t_m)^n,$$

where t_m is the time measured from the start of isothermal section as illustrated in Figure 5.

From the above two equations,

Table III. Sintering Kinetic parameters

Pellet	Isothermal Sintering Temperature [K (°C)]	n	$Q = 509 \text{ KJ/mol}$ $K' = 3.8 \times 10^{13} \text{ s}^{-1}$
P1	1423 (1150)	0.2403	
P2	1473 (1200)	0.2312	
P3	1523 (1250)	0.1900	
P3	1523 (1250)	0.2279	
P4	1573 (1300)	0.2632	
P4	1573 (1300)	0.2216	
P5	1623 (1350)	0.1934	

$$\ln\left(\frac{\gamma}{\gamma^*}\right) = n \ln\left(\frac{t^* + t_m}{t^*}\right). \quad [9]$$

Using the data of sintering ratios on the isothermal segment and Eq. [9], the parameters n and t^* were estimated using least square fit for different experiments. With these estimated parameters, Eq. [9] has been plotted for experiments with different sintering temperatures shown in Figure 6. The straight lines indicate that Eq. [7] is excellent in capturing the sintering kinetics. The slope of the straight lines gives the 'n' value. The values of n for different experiments are shown in Table III. The mean value of the n and its standard deviation were found to be 0.2099 and 2.57 pct, respectively.

Further, the values of K were estimated for sintering temperatures and Eq. [8] was used to estimate the values of K' and the activation energy Q . The plot showing the $1/T$ vs $\ln(KT^{1/n})$ is shown in Figure 7. Computed sintering kinetic parameters, namely, n , K' and Q are shown in Table III.

D. Sintering Prediction Using Kinetic Parameters

In the actual industrial induration process, sintering occurs under non-isothermal conditions. Variation of sintering ratio, γ , with time under isothermal condition described by Eq. [7] is extended to consider non-isothermal conditions using the following methodology.

Let γ_t and $\gamma_{t+\Delta t}$ denote the sintering ratios at time t and $t + \Delta t$, respectively, and corresponding temperatures be denoted by T_t and $T_{t+\Delta t}$. During this time interval Δt , let us say that sintering occurs isothermally at $T_{t+\Delta t}$ from γ_t to $\gamma_{t+\Delta t}$ (This is equivalent to discretizing the time-temperature plot with small isothermal steps). If so, the sintering during this time interval Δt can be written as

$$\gamma_{t+\Delta t} = K(T_{t+\Delta t}) \left(\left(\frac{\gamma_t}{K T_{t+\Delta t}} \right)^{1/n} + \Delta t \right)^n, \quad [10]$$

where $\left(\frac{\gamma_t}{K(T_{t+\Delta t})} \right)^{1/n}$ is the time that would have taken to achieve sintering ratio of γ_t isothermally at temperature $T_{t+\Delta t}$.

The variation of γ can be obtained by knowing the temporal variation of temperature and the correspond-

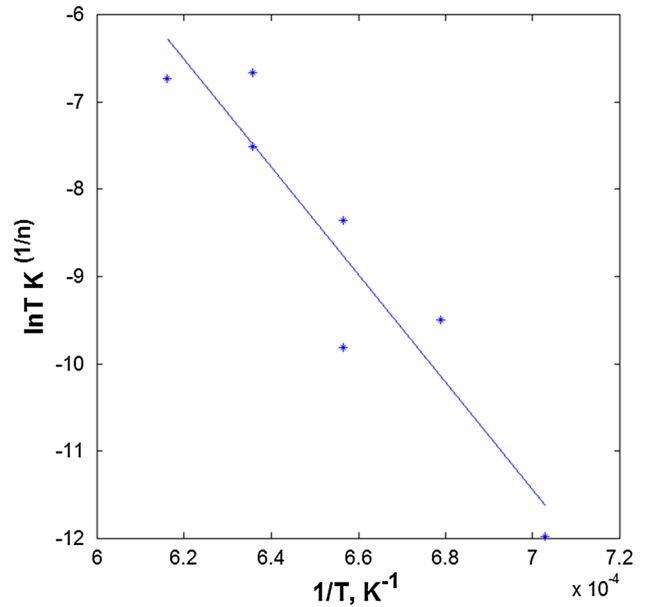


Fig. 7—Activation energy (Q) and rate constant (K') for sintering of oxidized magnetite pellets.

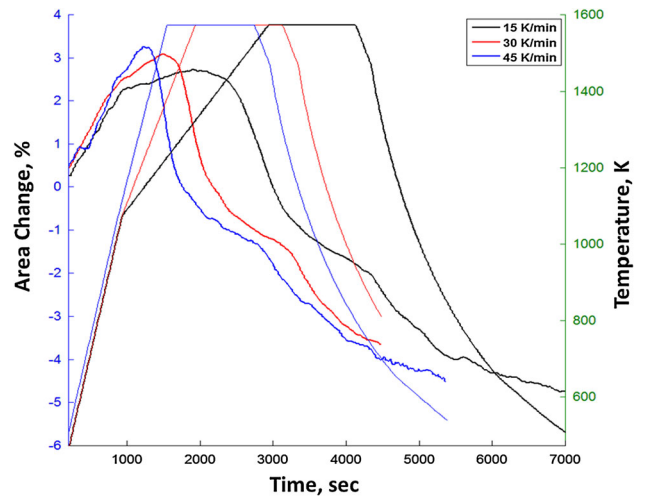


Fig. 8—Shrinkage curves for pellets exposed to different heating rates.

ing sintering rate constant, K , using Eq. [10] by marching in time for sufficiently small step of Δt .

Experiments have also been performed with pellets exposed to three different heating rates up to a temperature of 1573 K (1300 °C) in optical dilatometer to capture their shrinkage during induration as shown in Figure 8. It depicts that different heating rates have different shrinkage rates but similar degree of shrinkage at same temperature. These have further been utilized for the purpose of validating the predicted sintering behavior.

The predicted values are compared with those obtained from the experiments at different heating rates and are shown in Figure 9. It depicts the sintering state of pellet under variable heating rates which it experiences during complete induration cycle comprising non-

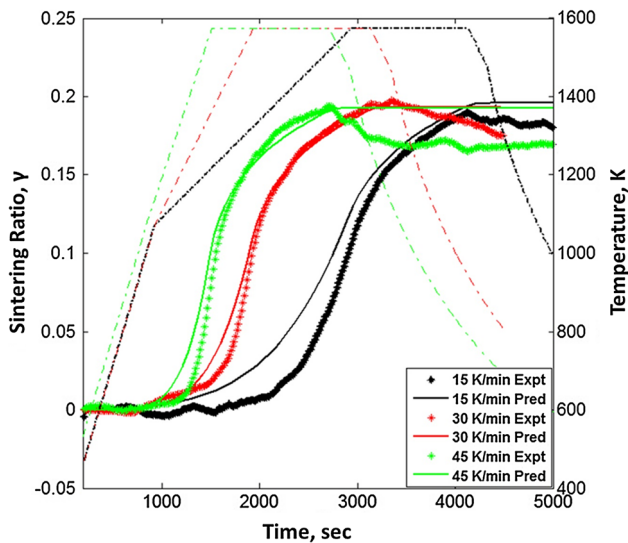


Fig. 9—Predicted and estimated sintering ratio for pellets exposed to different heating rates.

isothermal heating followed by isothermal and thereafter cooling. The predicted sintering states for the pellets are in quite good agreement with the experimental ones. This demonstrates that using the sintering kinetic parameters, namely, n , K' , and Q , it is possible to predict the extent of sintering for any non-isothermal profile using Eq. [10].

IV. CONCLUSIONS

The sintering kinetics of a single oxidized magnetite pellet has been experimentally investigated by capturing the *in situ* shrinkage of the pellet kept in a furnace. The shrinkage was captured using an optical dilatometer which unlike the traditional alumina push-rod dilatometer does not interfere with the process. Sintering, characterized through shrinkage, can be quantified using three kinetic parameters, namely activation energy (Q) and rate constant (K') and a time exponent (n). These kinetic parameters were deduced from shrinkage data under isothermal conditions. For the oxidized magnetite pellets studied in the current work, the activation energy Q was found to be 509 kJ/mol. A methodology was developed to predict the extent of sintering under non-isothermal condition using the above kinetic parameters. These predictions were validated using experimental data.

Quantitative description of sintering in iron ore pellets can not only be useful in predicting the state of the pellet during industrial induration process but also help in optimizing the appropriate raw material mix for making pellets.

ACKNOWLEDGMENTS

Authors thank the Hjalmar Lundbohm Research Centre (HLRC) for their financial support. We also

thank Ola Eriksson, Daniel Marjavaara, Gustaf Magnusson, Anders Dahlin, Axel Stahlstrom, Klauss Weigel, and Kjell-Ove Mickelsson of LKAB for their technical support. We also thank Prof. N. B. Ballal and Prof. M. P. Gururajan of Indian Institute of Technology (IIT) Bombay for valuable discussions.

NOMENCLATURE

$\delta_{A,overall}$	Overall percentage area change at any instant during induration
$\delta_{A,sintering}$	Percentage area change due to sintering any instant during induration
δ_A	Percentage area change at any instant
$\delta_{A,true}$	Percentage area change when pellet has no pores
α	Volumetric thermal coefficient of expansion
β	Area thermal coefficient of expansion
V_0	Initial volume of a material
V	Volume of material at any temperature
V_{true}	Volume of the pellet if it would have undergone complete sintering with no pores
T_0	Initial temperature
T	Temperature at any instant
γ	Sintering ratio of the pellet
γ^*	Sintering ratio at the start of the isothermal section
ρ	Bulk density of the pellet at any instant
ρ_{true}	True density of the pellet
ρ_0	Initial bulk density of pellet
t	Time for sintering reaction
t^*	Time corresponds if the pellet had attained a sintering ratio of γ^* from the start under isothermal condition
t_m	Measured time in isothermal section
n	Time exponent
K	Reaction rate constant
Q	Activation energy
R	Universal gas constant
γ_t	Sintering ratio at time t
$\gamma_{t+\Delta t}$	Sintering ratio at time $t + \Delta t$
T_t	Temperature at time t
$T_{t+\Delta t}$	Temperature at time $t + \Delta t$
$K(T_{t+\Delta t})$	Rate constant at $t + \Delta t$

REFERENCES

1. S.P.E. Forsmo, S. Forsmo, P. Samskog, and B.M.T. Björkman: *Powder Technol.*, 2008, vol. 183, pp. 247–59.
2. S.R. Cooke and W.F. Stowasser, Jr: *Trans. AIME*, 1952, vol. 193, pp. 1223–30.
3. V. Niiniskorpi: *Ironmaking Conference Proceedings*, 2001, pp. 767–80.
4. M. Tang, H.J. Cho, and P.C. Pistorius: *Metall. Mater. Trans. B*, 2014, vol. 45 B, pp. 1304–14.
5. J.R. Wynnycyk and W.A. McCurdy: *Metall Trans*, 1974, vol. 5, pp. 2207–15.
6. P. Semberg, A. Rutqvist, C. Andersson, and B. Björkman: *ISIJ Int.*, 2011, vol. 51, pp. 173–80.

7. J. Thurlby, R. Batterham, and R. Turner: *Int. J. Miner. Process.*, 1979, vol. 6, pp. 43–64.
8. J. Thurlby: *Metall. Trans. B*, 1988, vol. 19B, pp. 103–12.
9. R. Davis: *Can. J. Chem. Eng.*, 1996, vol. 74, pp. 1004–09.
10. M. Cross and P. Blot: *Metall. Mater. Trans. B*, 1999, vol. 30B, pp. 803–13.
11. S. Sadrnezhad, A. Ferdowsi, and H. Payab: *Comput. Mater. Sci.*, 2008, vol. 44, pp. 296–02.
12. M. Barati: *Int. J. Miner. Process.*, 2008, vol. 89, pp. 30–39.
13. R.L. Coble: *J. Am. Ceram. Soc.*, 1958, vol. 41, pp. 55–62.
14. D.L. Johnson and I.B. Cutler: *J. Am. Ceram. Soc.*, 1963, vol. 46, pp. 545–50.
15. W.S. Young and I.B. Cutler: *J. Am. Ceram. Soc.*, 1970, vol. 53, pp. 659–63.
16. J.D. Hansen, R.P. Rusin, M. Teng, and D.L. Johnson: *J. Am. Ceram. Soc.*, 1992, vol. 75, pp. 1129–35.
17. J. M'Peko, A.R. Ruiz-Salvador, and G. Rodriguez-Fuentes: *Mater. Lett.*, 1998, vol. 36, pp. 290–93.
18. M. Nikolić, N.J. Labus, and M.M. Ristić: *Sci. Sinter.*, 2005, vol. 37, pp. 19–25.
19. A.K. Burnham: *Chem. Eng. J.*, 2005, vol. 108, pp. 47–50.
20. V. Pouchly and K. Maca: *Sci. Sinter.*, 2010, vol. 42, pp. 25–32.
21. D. Kosanović, S. Filipović, N. Obradović, V. Pavlović, and M. Ristić: *J. Appl. Eng. Sci.*, 2011, vol. 9, pp. 317–22.
22. W. Zeng, L. Gao, L. Gui, and J. Guo: *Ceram. Int.*, 1999, vol. 25, pp. 723–26.
23. Z.Y. Liu, N.H. Loh, K.A. Khor, and S.B. Tor: *Scripta Mater.*, 2001, vol. 44, pp. 1131–37.
24. P. Dehaut, L. Bourgeois, and H. Chevrel: *J. Nucl. Mater.*, 2001, vol. 299, pp. 250–59.
25. Z. Holková, L. Pach, V. Kovár, and S. Svetík: *Ceram. Silik.*, 2003, vol. 47, pp. 13–19.
26. T. Kuttly, K. Khan, P. Hegde, A. Sengupta, S. Majumdar, and H. Kamath: *Sci. Sinter.*, 2003, vol. 35, pp. 125–32.
27. T. Fang, J. Shiue, and F. Shiau: *Mater. Chem. Phys.*, 2003, vol. 80, pp. 108–13.
28. D. Lahiri, S. Rao, G. Rao, and R. Srivastava: *J. Nucl. Mater.*, 2006, vol. 357, pp. 88–96.
29. D. Blaine, J. Gurosik, S. Park, D. Heaney, and R. German: *Metall. Mater. Trans. A*, 2006, vol. 37A, pp. 715–20.
30. K.G. Ewsuk, D.T. Ellerby, and C.B. DiAntonio: *J. Am. Ceram. Soc.*, 2006, vol. 89, pp. 2003–09.
31. M. Mazaheri, F. Golestani-Fard, and A. Simchi: *10th International Conference and Exhibition of the European Ceramic Society*, Berlin, 2007.
32. A. Karamanov, B. Dzhantov, M. Paganelli, and D. Sighinolfi: *Thermochim. Acta*, 2013, vol. 553, pp. 1–7.
33. R.M. German: *Sintering Theory and Practice*, Wiley Interscience, New York, 1996, vol. 1, pp. 67–41.
34. M.V. Nikolić, V.P. Pavlović, V.B. Pavlović, N. Labus, and B. Stojanović: *Mater. Sci. Forum*, 2005, vol. 494, pp. 417–22.
35. M. Gasik, A. Keski-Honkola, and Y. Bilotsky: *17th Plansee Seminar*, 2009, vol. 1, pp. 70/1–70/10.
36. J.R. Wynnyckyj and T.Z. Fahidy: *Metall. Trans.*, 1974, vol. 5, pp. 991–1000.
37. S. Forsmo: Ph.D. Thesis, Lulea University of Technology, Lulea, 2007.
38. D.R. Gaskell: *Introduction to the Thermodynamics of Materials*, 5th ed., CRC Press, New York, 2008, p. 6.